15th World Congress on Computational Mechanics (WCCM-XV)
8th Asian Pacific Congress on Computational Mechanics (APCOM-VIII)
Virtual Congress: 31 July – 5 August 2022
S. Koshizuka (Ed.)

THREE-DIMENSIONAL SUPER-RESOLUTION OF PASSIVE-SCALAR AND VELOCITY DISTRIBUTIONS USING NEURAL NETWORKS FOR REAL-TIME PREDICTION OF URBAN MICROMETEOROLOGY

YUKI YASUDA[1], RYO ONISHI[1] AND KEIGO MATSUDA[2]

[1] Tokyo Institute of Technology
2-12-1 Ookayama, Meguro-ku, Tokyo 1528550, Japan
yasuda.y.aa@m.titech.ac.jp, onishi.ryo@gsic.titech.ac.jp

[2] Japan Agency for Marine-Earth Science and Technology
3173-25 Showa-machi, Kanazawa-ku, Yokohama, Kanagawa 2360001, Japan
k.matsuda@jamstec.go.jp

Key words: Building-Resolving Micrometeorological Simulations, Three-Dimensional Super-Resolution, Neural Networks, Real-Time Prediction

Abstract. *In future cities, micrometeorological predictions will be essential to various services such as drone operations. However, the real-time prediction is difficult even by using a super-computer. To reduce the computation cost, super-resolution (SR) techniques can be utilized, which infer high-resolution images from low-resolution ones. The present paper confirms the validity of three-dimensional (3D) SR for micrometeorology prediction in an urban city. A new neural network is proposed to simultaneously super-resolve 3D temperature and velocity fields. The network is trained using the micrometeorology simulations that incorporate the buildings and 3D radiative transfer. The error of the 3D SR is sufficiently small: 0.14 K for temperature and 0.38 m s^{-1} for velocity. The computation time of the 3D SR is negligible, implying the feasibility of real-time predictions for the urban micrometeorology.*

1 INTRODUCTION

In future cities, various IoT devices will constantly access meteorological data and social network information on cloud networks. Each system using IoT devices will provide a variety of services in response to complex changes in weather and society without people being aware of it. Such social services will require real-time predictions of urban micrometeorology.

The authors' research group has developed a micrometeorological model that can resolve buildings and tree canopies at several meter resolution in urban areas (e.g., [1, 2, 3, 4]). However, the computational cost of such simulations is high, and the real-time prediction is difficult even with a supercomputer.

Super-resolution (SR) refers to methods of estimating high-resolution (HR) images from those with low-resolution (LR). SR is studied in computer vision as an application of neural networks (NNs) (e.g., [5, 6]). The success of such NNs has resulted in an increased number of studies that focus on the SR in fluid mechanics (e.g., [7, 8, 9, 10]). Onishi et al. (2019) [10] proposed the super-resolution simulation system using NN, where HR inferences are obtained with an NN from the LR results of micrometeorology simulations. Once the NN is trained, it can make inferences at low computational cost, which would make the real-time prediction possible.

The authors demonstrated the feasibility of super-resolution simulations for two-dimensional (2D)

temperature [10, 11]. The three-dimensional (3D) flow field is necessary for its own application, but may also be essential to make an overall inference more physically valid because 3D velocity advects scalars such as temperature. The SR of 3D flow fields has been studied using NNs (e.g., [12, 13]); however, most studies discuss canonical flows such as channel turbulence. Thus, the effectiveness of 3D SR for complex flows in urban areas has not been validated.

This research aims to confirm the validity of 3D SR for micrometeorology simulations in urban cities. The following things are demonstrated:

- The 3D SR of temperature is as accurate as the 2D SR, even though 3D SR is generally more difficult.
- Not only temperature but also velocity can be super-resolved with high accuracy in 3D.
- The computation time of the 3D SR is sufficiently short, implying the feasibility of real-time predictions.

The remaining paper is organized as follows. Section 2 describes the NNs for the 2D and 3D SR. Section 3 gives the methods of training the NNs utilizing the data of the micrometeorology simulations in Tokyo, Japan. Section 4 analyzes the results of the 2D and 3D SR. The conclusions are presented in Section 5.

2 CONVOLUTIONAL NEURAL NETWORKS

This section describes the convolutional neural networks (CNNs) of the 2D and 3D SR. The former and latter are referred to as 2dSR-Net and 3dSR-Net, respectively. The 2dSR-Net has been proposed in the authors' previous study [11], which super-resolves only the 2D temperature. In contrast, the 3dSR-Net simultaneously super-resolves temperature and velocity.

2.1 Two-dimensional super-resolution network (2dSR-Net)

The 2dSR-Net [11] is based on the two CNNs [14, 15]. The network architecture is shown in Fig. 1. The output is the 2D temperature in the HR. The input consists of temperature, horizontal velocity, building height, and downward shortwave radiation on the surface. The temperature and horizontal velocity are in the LR, whereas the building height and shortwave radiation are in the HR. To align the resolution, the bicubic interpolation is applied to the LR inputs. The temperature and velocity are originally 3D fields from micrometeorology simulations, and the 2D fields are obtained from the grids near the bottom surface.

The 2dSR-Net consists of three parts (Fig. 1): encoder, nonlinear mapping, and decoder. The encoder separately converts each input of physics quantities into features. The nonlinear mapping contains an attention module named the squeeze-and-excitation block [15]. This module gives a weight to each feature, and this weight is multiplied to all pixel values of the feature. Finally, the decoder reconstructs the HR temperature using the skip connection. The skip connection directly connects the input to the output, allowing the 2dSR-Net to learn the difference between the HR and LR temperature.

2.2 Three-dimensional super-resolution network (3dSR-Net)

The 3dSR-Net is based on U-Nets [16, 17]. The network architecture is shown in Fig. 2. The output is the 3D temperature and velocity fields in the HR. The input is composed of the 3D temperature and velocity in the LR and the building mask in the HR. To align the resolution, the nearest-neighbor interpolation is applied to the LR inputs. The building mask takes 0 or 1, where it is 0 if a voxel, 3D version

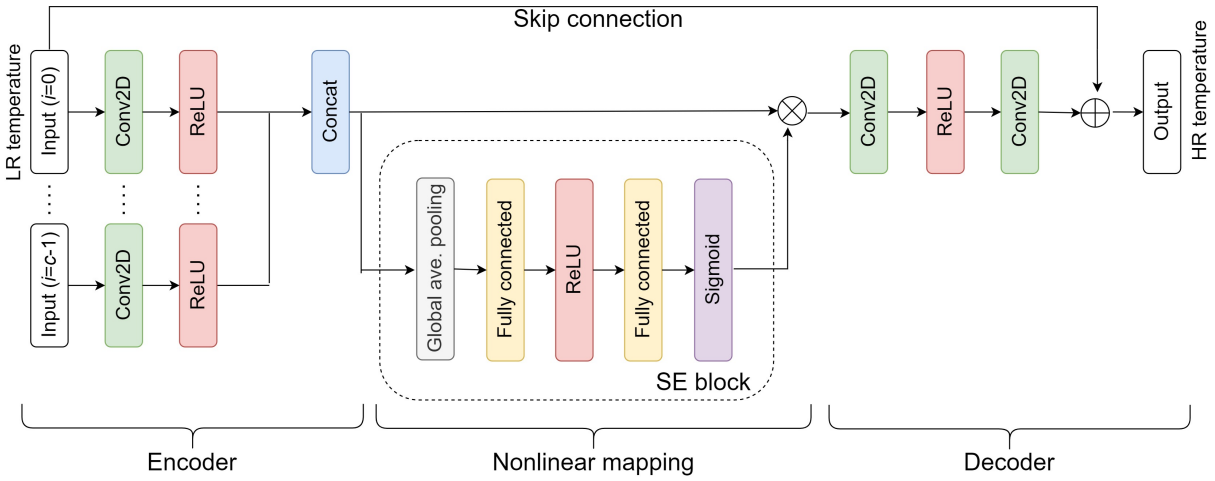

Figure 1: Network architecture of two-dimensional super-resolution net (2dSR-Net).

of pixel, is inside the building and otherwise 1.

The 3dSR-Net has the shape of U, consisting again of three parts (Fig. 2): encoder, nonlinear mapping, and decoder. The encoder reduces the input size by convolutions and extracts the reduced-order features. These features are mapped nonlinearly and passed to the decoder. The decoder restores the features to the original size using upsampling algorithms. Here, a 3D version of the pixel shuffle [18] is employed. The skip connection directly connects the feature in each resolution from the encoder to the decoder, allowing the 3dSR-Net to reconstruct the difference between the HR and LR fields. The building mask is fed into each block, where the resolution is adjusted using the spatial average.

3 METHODOLOGY

The 2dSR- and 3dSR-Nets were trained using the results of the micrometeorology simulations in Tokyo, Japan. Section 3.1 briefly gives the configuration of the simulations. Section 3.2 describes the training methods.

3.1 Micrometeorology simulations

This paper employs a multi-scale atmosphere-ocean coupled model named the Multi-Scale Simulator for the Geoenvironment (MSSG) [1, 2, 3, 4]. MSSG covers global, meso-, and urban scales. For urban scales, the atmospheric component of MSSG is used as a building-resolving large-eddy simulation (LES) model, which can be coupled with a 3D radiative transfer model [4]. The governing equations are the conservation equations of mass, momentum, and energy for compressible flows as well as the transport equations for mixing ratios of water substances including water vapor, liquid, and ice cloud particles. A detailed description of the numerical parameters is found in precursor studies [4, 10].

The domain of Tokyo is centered at 35.680882°N and 139.767019°E (Fig. 3). The horizontal size is 2 km $\times$ 2 km with the 5-m resolution, and the vertical size is 1,500 m spanned by the 151 stretched grids. This domain is embedded in the nested mesoscale simulation domains. Specifically, the mesoscale simulations adopt three two-way-coupled nested systems as shown in Fig. 3 (Domains 1 to 3). The boundary and initial conditions of the mesoscale simulations were taken from the Japan Meteorological

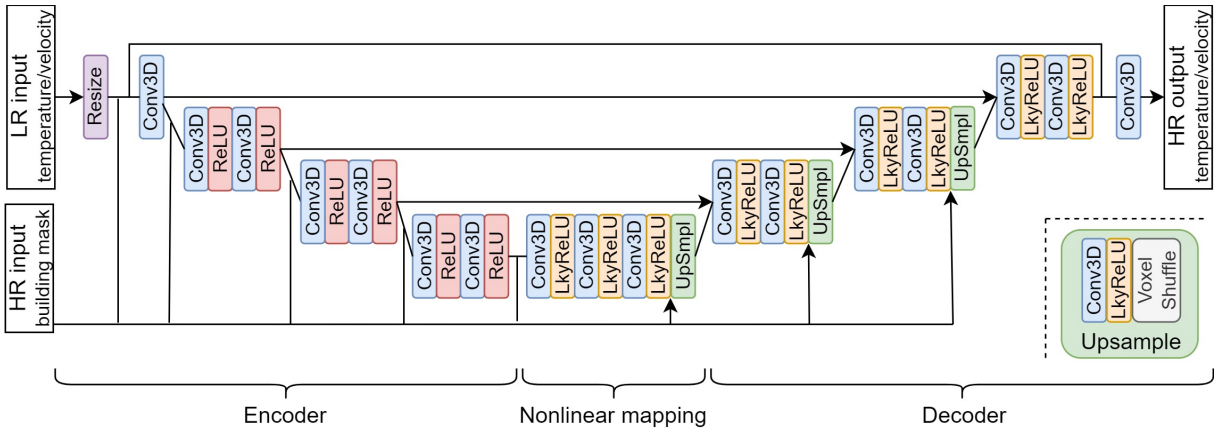

Figure 2: Network architecture of three-dimensional super-resolution net (3dSR-Net). The label LkyReLU and Upsmpl means Leaky ReLU and Upsample, respectively.

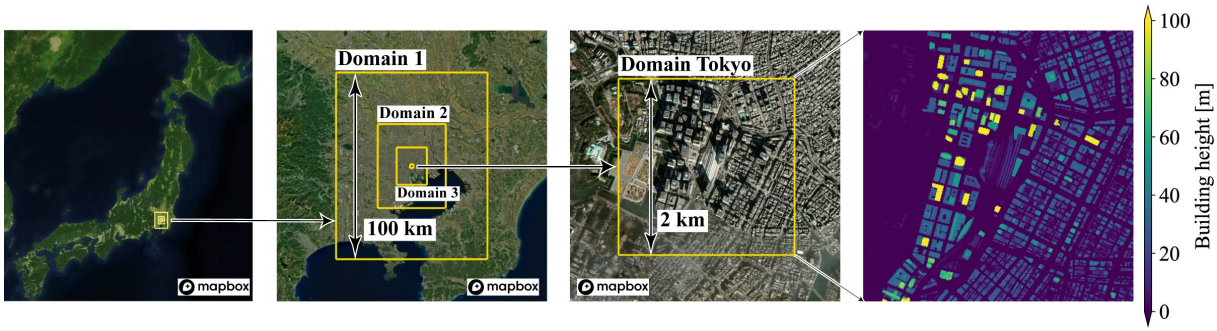

Figure 3: Domains of mesoscale and large-eddy simulations around Tokyo, Japan. The rightest figure shows the building height distribution in Domain Tokyo.

Agency (JMA) mesoscale analysis data (MANAL) [19], while those of the LESs were obtained from the mesoscale simulations of Domain 3. To focus on heat mitigation, extremely hot days were selected with the maximum temperature that exceeded 35°C. The 85 LESs were conducted between 2013 and 2015 for the 2D SR experiment, and the 57 LESs between 2013 and 2020 were performed for the 3D SR. The integration time of each LES was one hour, where the first 10-min data were discarded and the rest of 50 min were used to obtain the 1-min-averaged fields.

3.2 Training methods of neural networks

The 2dSR- and 3dSR-Nets were trained with the pairs of the LR and HR data. All HR fields were generated from the LESs described in the previous subsection. All LR fields were obtained by spatially averaging the HR ones, where the window size was four in all directions. Thus, the resolution of LR data is four times lower than that of HR data both in 2D and 3D. In 3D, the LR fields have value only outside the LR buildings where the LR building mask is equal to 1. This mask was obtained from the LR building height. This LR building height was calculated with the spatial average as well and will be used in actual LR micrometeorology simulations.

Adam optimizer was employed in training the NNs. The loss function was the mean squared error for the 2dSR-Net, while it was the L1 loss for the 3dSR-Net.

All data were first sorted in chronological order, with the first 60% as training data, the next 20% as validation data, and the last 20% as test data. In the 2D SR experiment, the training was finished by early stopping with the patience parameter of 300 epochs. On the other hand, in the 3D SR experiment, the training was ended at the 600th epoch, and the model weights giving the lowest validation loss were recorded.

4 RESULTS

This section evaluates the 2dSR- and 3dSR-Nets using the test data, which are not used in training. Section 4.1 discusses the result of the 2D SR of temperature. The 2D SR exhibits the sufficiently accurate inference [11]. Section 4.2 demonstrates that the 3D SR of temperature is as accurate as the 2D SR. Furthermore, the SR of velocity is examined, as the 3dSR-Net simultaneously super-resolves temperature and velocity.

4.1 Two-dimensional super-resolution

The inference of the 2D SR is compared with a baseline of the bicubic interpolation. Figure 4 shows an example of the SR of temperature. The 2dSR-Net reconstructs a temperature field similar to the ground truth and greatly reduces the error near the building walls. In contract, the temperature field given by the bicubic interpolation is blurred, and the error is larger than that of the 2dSR-Net.

Table 1 compares the root-mean-squared error of the 2dSR-Net with that of the bicubic interpolation. The previous studies of LESs [20, 4] indicate that a required precision in the SR would be around 0.2 K. The 2dSR-Net exhibits the error lower than this criterion: 0.146 K. The 2dSR-Net does not infer velocity components, and the error values are blank for velocity in Table 1.

Table 1: Errors of super-resolved quantities. The symbol ΔT denotes the error in temperature, and Δu, Δv, and Δw are the errors in eastward, northward, and vertical components of velocity, respectively.

Method	ΔT [K]	Δu [m s^{-1}]	Δv [m s^{-1}]	Δw [m s^{-1}]
Bicubic interpolation	0.279	–	–	–
2dSR-Net	0.146	–	–	–
3dSR-Net	0.139	0.343	0.382	0.213

4.2 Three-dimensional super-resolution

The 3dSR-Net simultaneously super-resolves temperature as well as velocity. Figure 5 shows an example of the 3D SR at two altitude levels (5 and 25 m). The white areas denote the interior of the buildings, where all physics quantities have no value. The building shape depends on the resolution. Narrow streets between buildings are not represented in the LR, resulting in the increase of the white areas. This means that the volume of flow fields available for inference is reduced in the LR. Nonetheless, all super-resolved fields are similar to the ground truth: the temperature and velocity distributions are successfully reconstructed even between the buildings [Fig. 5(a)]. This result suggests that the pattern matching between the LR and HR is efficiently utilized in the 3D SR among temperature and velocity. Note that the pattern

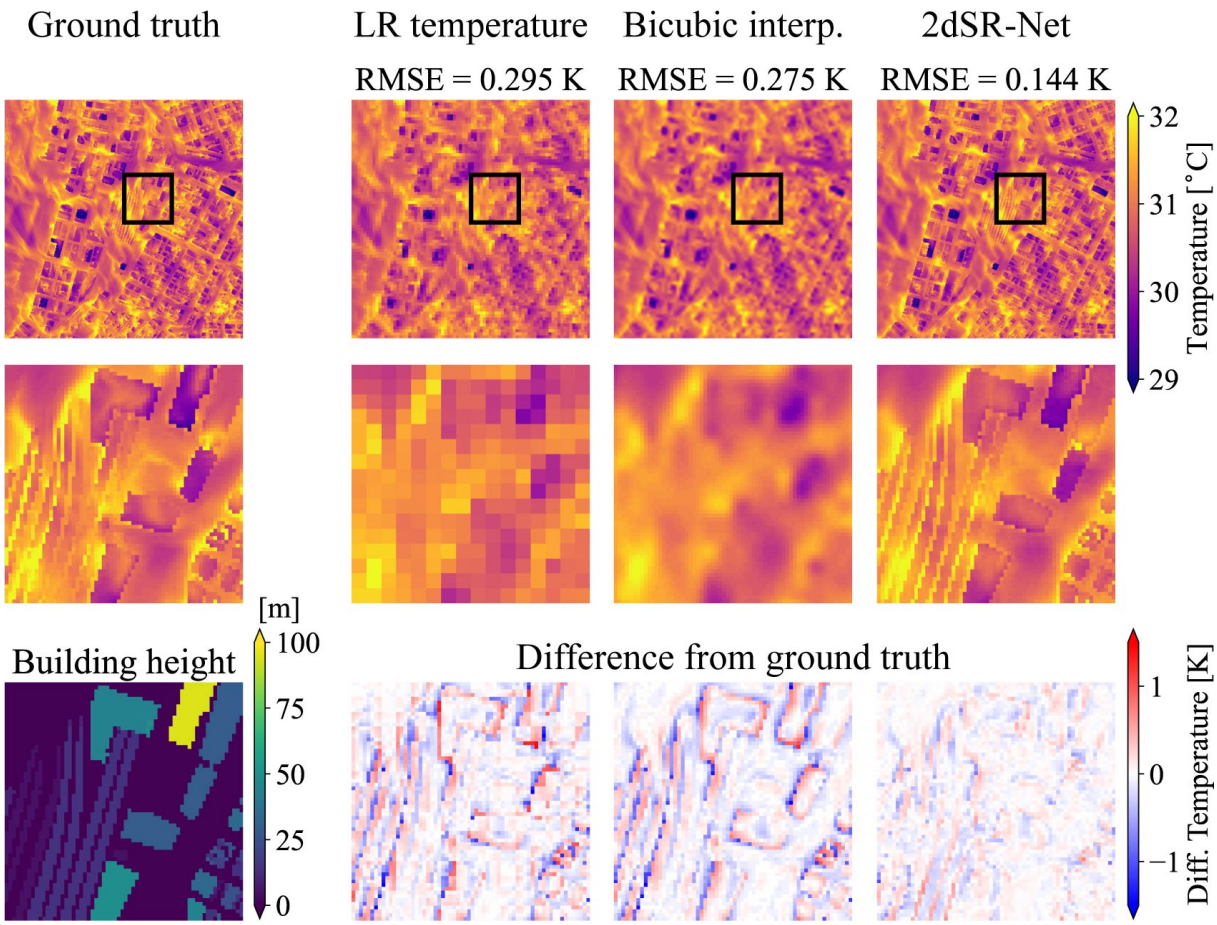

Figure 4: An example of the 2D super-resolution of temperature. The images in the second and third rows focus on the rectangular areas in the first row.

matching is also referred to as the sparse-coding-based method (e.g., [14]). The error is larger near the ground [Fig. 5(a)] and is reduced as the altitude becomes high [Fig. 5(b)]. This result is likely due to a reduction in the number of grids inside the buildings at a higher altitude, which makes the 3D SR easier.

Table 1 shows the L1 loss of the 3dSR-Net for temperature and velocity. The altitude where the loss is the largest was selected to each quantity, and its loss value is listed in Table 1. The accuracy of the 3D SR of temperature is comparable to that of the 2D SR, even though 3D SR is generally more difficult. Note that the training dataset comprises more micrometeorology simulations in the 2D SR (51 runs) than in the 3D SR (33 runs). The simultaneous SR of temperature and velocity might have reduced the error because velocity advects temperature and the velocity distribution may be useful to infer the temperature. The errors of the velocity components are also displayed in Table 1. All velocity errors are smaller than 0.4 m s^{-1}. When all quantities are non-dimensionalized, the velocity errors are comparable to the temperature error, implying that the accuracy of the 3D SR of velocity is sufficiently high.

The total computation time is estimated to examine the possibility of real-time predictions. The one-hour HR micrometeorology simulation takes around 8 hours using a super-computer. The computation time of the LR counterpart is estimated at approximately 2 minutes. This LR simulation will generate 60

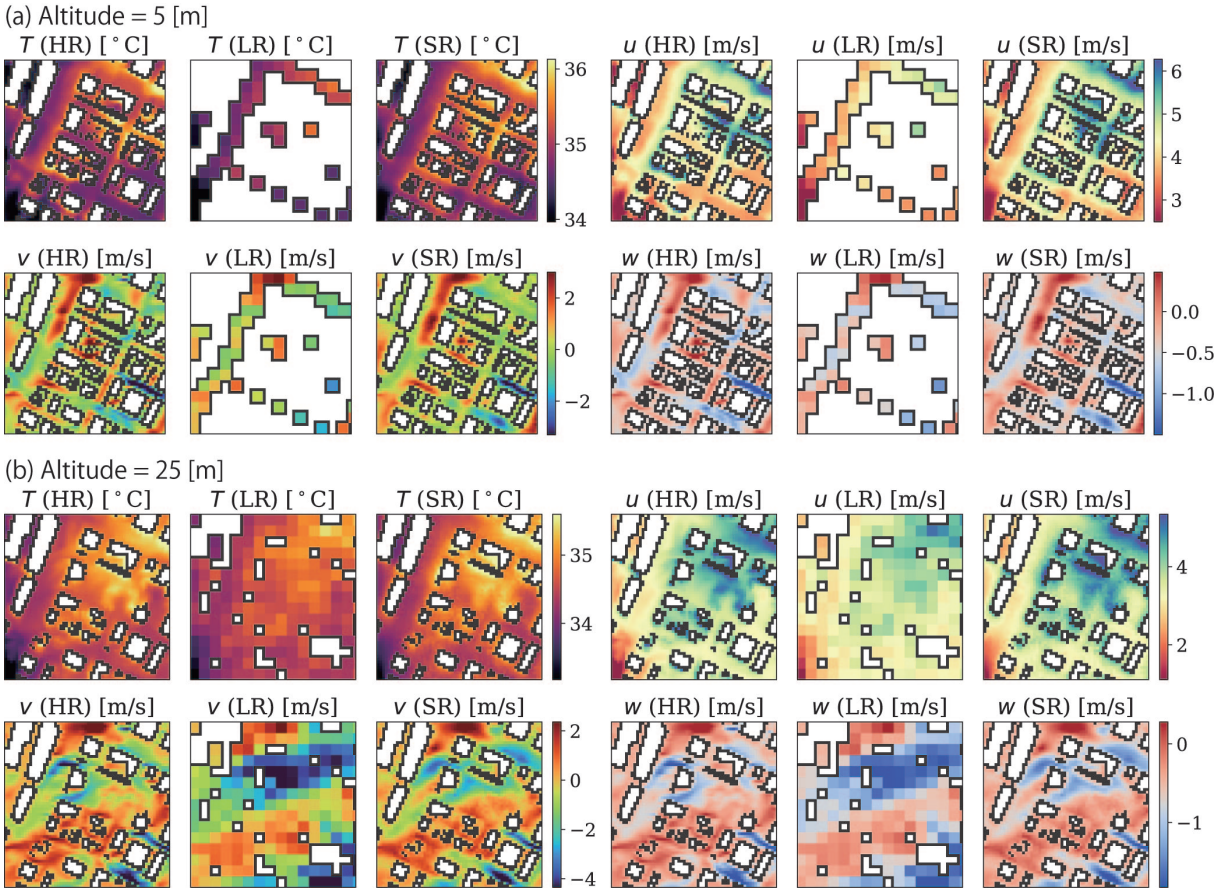

Figure 5: An example of the 3D super-resolution of temperature and velocity. The altitude is (a) 5 m and (b) 25 m from the ground. The labels HR, LR, and SR mean high-resolution, low-resolution, and super-resolution, respectively. The symbol T denotes temperature, and u, v, and w are eastward, northward, and vertical components of velocity, respectively.

sets of 1-min-averaged 3D data. The SR of these data takes about 20 seconds using an NVIDIA A100 40GB PCIe GPU board. Therefore, the total computation time to make a one-hour simulation is less than 3 minutes. This estimation implies the feasibility of real-time predictions using the super-resolution simulation system [10].

5 CONCLUSIONS

The present paper has confirmed the validity of 3D SR for micrometeorology simulations in Tokyo, Japan. A new neural network has been proposed to simultaneously super-resolve 3D temperature and velocity fields. The network was trained using the micrometeorology simulations that incorporated the buildings and 3D radiative transfer. The 3D SR of temperature is as accurate as the 2D SR, even though 3D SR is generally more difficult. The result indicates that the pattern matching between the LR and HR is efficiently utilized in the 3D SR among temperature and velocity. Not only temperature but also velocity can be super-resolved with high accuracy. The computation time of the 3D SR is sufficiently

short: it takes about three minutes to obtain a one-hour simulation result. This estimation implies the feasibility of real-time predictions for the urban micrometeorology.

There are at least two directions to future work. The first is the investigation of generalizability. The 2D SR is possible in another city that is not used to generate the training data [11]. It is not clear whether similar results are obtained for the 3D SR. The second is the incorporation of physics loss such as the residual of the continuity equation. Several studies indicate that the accuracy is enhanced when a physics loss is taken into account (e.g., [21, 13]). It will be a first step to include the residual of the continuity equation and to investigate a change in accuracy for the 3D SR.

Acknowledgements

This work was supported by the JSPS KAKENHI (grant numbers 20H05751 and 20H02074). The building-resolving micrometeorology simulations and deep learning were performed on the Earth Simulator system of the Japan Agency for Marine-Earth Science and Technology (JAMSTEC).

REFERENCES

[1] K. Takahashi, R. Onishi, Y. Baba, S. Kida, K. Matsuda, K. Goto, and H. Fuchigami, "Challenge toward the prediction of typhoon behaviour and down pour," *Journal of Physics: Conference Series*, vol. 454, p. 012072, 8 2013.

[2] R. Onishi and K. Takahashi, "A warm-bin–cold-bulk hybrid cloud microphysical model*," *Journal of the Atmospheric Sciences*, vol. 69, pp. 1474–1497, 5 2012.

[3] W. Sasaki, R. Onishi, H. Fuchigami, K. Goto, S. Nishikawa, Y. Ishikawa, and K. Takahashi, "Mjo simulation in a cloud-system-resolving global ocean-atmosphere coupled model," *Geophysical Research Letters*, vol. 43, pp. 9352–9360, 2016.

[4] K. Matsuda, R. Onishi, and K. Takahashi, "Tree-crown-resolving large-eddy simulation coupled with three-dimensional radiative transfer model," *Journal of Wind Engineering and Industrial Aerodynamics*, vol. 173, pp. 53–66, 2 2018.

[5] V. K. Ha, J.-C. Ren, X.-Y. Xu, S. Zhao, G. Xie, V. Masero, and A. Hussain, "Deep learning based single image super-resolution: A survey," *International Journal of Automation and Computing*, 2019.

[6] S. Anwar, S. Khan, and N. Barnes, "A deep journey into super-resolution: A survey," *ACM Comput. Surv.*, vol. 53, may 2020.

[7] T. Vandal, E. Kodra, S. Ganguly, A. Michaelis, R. Nemani, and A. R. Ganguly, "Deepsd: Generating high resolution climate change projections through single image super-resolution," pp. 1663–1672, Association for Computing Machinery, 2017.

[8] Y. Xie, E. Franz, M. Chu, and N. Thuerey, "Tempogan: A temporally coherent, volumetric gan for super-resolution fluid flow," *ACM Trans. Graph.*, vol. 37, 7 2018.

[9] K. Fukami, K. Fukagata, and K. Taira, "Super-resolution reconstruction of turbulent flows with machine learning," *Journal of Fluid Mechanics*, vol. 870, pp. 106–120, 7 2019.

[10] R. Onishi, D. Sugiyama, and K. Matsuda, "Super-resolution simulation for real-time prediction of urban micrometeorology," *SOLA*, vol. 15, pp. 178–182, 2019.

[11] Y. Yasuda, R. Onishi, Y. Hirokawa, D. Kolomenskiy, and D. Sugiyama, "Super-resolution of near-surface temperature utilizing physical quantities for real-time prediction of urban micrometeorology," *Building and Environment*, vol. 209, p. 108597, 2022.

[12] K. Fukami, K. Fukagata, and K. Taira, "Assessment of supervised machine learning methods for fluid flows," *Theoretical and Computational Fluid Dynamics*, vol. 34, pp. 497–519, 2020.

[13] M. Bode, M. Gauding, Z. Lian, D. Denker, M. Davidovic, K. Kleinheinz, J. Jitsev, and H. Pitsch, "Using physics-informed enhanced super-resolution generative adversarial networks for subfilter modeling in turbulent reactive flows," *Proceedings of the Combustion Institute*, vol. 38, pp. 2617–2625, 1 2021.

[14] C. Dong, C. C. Loy, K. He, and X. Tang, "Learning a deep convolutional network for image super-resolution," in *Computer Vision – ECCV 2014* (D. Fleet, T. Pajdla, B. Schiele, and T. Tuytelaars, eds.), (Cham), pp. 184–199, Springer International Publishing, 2014.

[15] J. Hu, L. Shen, and G. Sun, "Squeeze-and-excitation networks," pp. 7132–7141, 2018.

[16] L. Schweri, S. Foucher, J. Tang, V. C. Azevedo, T. Günther, and B. Solenthaler, "A physics-aware neural network approach for flow data reconstruction from satellite observations," *Frontiers in Climate*, vol. 3, 2021.

[17] O. Ronneberger, P. Fischer, and T. Brox, "U-net: Convolutional networks for biomedical image segmentation," in *Medical Image Computing and Computer-Assisted Intervention – MICCAI 2015* (N. Navab, J. Hornegger, W. M. Wells, and A. F. Frangi, eds.), (Cham), pp. 234–241, Springer International Publishing, 2015.

[18] W. Shi, J. Caballero, F. Huszar, J. Totz, A. P. Aitken, R. Bishop, D. Rueckert, and Z. Wang, "Real-time single image and video super-resolution using an efficient sub-pixel convolutional neural network," in *Proceedings of the IEEE Conference on Computer Vision and Pattern Recognition (CVPR)*, June 2016.

[19] J. M. Agency, "Japan meteorological agency mesoscale analysis data."

[20] Y. S. Liu, S. G. Miao, C. L. Zhang, G. X. Cui, and Z. S. Zhang, "Study on micro-atmospheric environment by coupling large eddy simulation with mesoscale model," *Journal of Wind Engineering and Industrial Aerodynamics*, vol. 107-108, pp. 106–117, 8 2012.

[21] C. Wang, E. Bentivegna, W. Zhou, L. Klein, and B. Elmegreen, "Physics-informed neural network super resolution for advection-diffusion models," in *Third Workshop on Machine Learning and the Physical Sciences (NeurIPS 2020)*, 2020.